Novel distributed coordination control for DC microgrid: Modeling, Analysis and Optimization

I. Mexis[a,*], H. Heo[a]

[a] *Aalborg University, School of Engineering and Science, Pontoppidanstræde 111, DK-9220 Aalborg East, Denmark*

Abstract

In the context of this paper, the hierarchical control structure of an islanded DC Micro-Grid (MG) system is implemented, based on which both primary and secondary control are applied. A detailed model of the inner control loops, droop control and general DC MG topology is derived. The sensitivity of different system structure and control parameters is analyzed. Furthermore, the tradeoffs between accurate current sharing and voltage regulation are examined, which acts as a guideline for the design of MG structure and its control parameters. Simulations about the traditional secondary controller are realized, based on which the containment and consensus-based algorithm are designed. Novel containment-based controller is proposed to control the voltage into a reasonable range and dynamic-consensus-based controller is used to achieve relative accurate current sharing. Finally, the designed controller is verified through simulations in MATLAB.

Keywords: DC Micro-Grid, droop control, secondary control, containment-based algorithm, current sharing

1. Introduction

DC microgrids are defined as local networks integrating various energy sources interfaced with power converters and feeding loads that are connected via DC power lines. The DC nature of emerging renewable sources(e.g. solar) and storage units(batteries, ultracapacitors) make them the most efficient and easiest solution since redundant conversion stages can be avoided. Nowadays, there is an increasing trend in the use of DC systems in residential, commercial and industrial systems. Typical applications are data centers and telecommunication central offices. Examples of loads that utilize DC voltage are ICT equipment, lighting, consumer electronics, white goods and electric vehicles. Compared to their AC counterparts, they present a series of advantages, i.e. in DC MGs there is no presence of reactive power, frequency synchronization issues, harmonics and transformer inrush current. Therefore, higher power quality can be obtained and the overall system's efficiency and availability are increased [1].

Similar to the control hierarchy of the legacy grid, a hierarchical control structure is conventionally adopted for MG operation, consisting of the tertiary, secondary and primary control [2]. The highest level, i.e. the tertiary control level, is beyond the scope of this paper and the focus is put on the other two control levels. The two main control objectives of DC MGs that such controllers should satisfy are the voltage regulation and the proportional current sharing. The microgrid voltage should not deviate from its nominal value more than a certain limit(typically 1%) and the converters should share their output current proportionally according to their capabilities.

Droop control is the most widely employed decentralized method in order to achieve proportional current sharing. This can be realized by linearly reducing the voltage reference as the output current increases [2]. However, there are two limitations regarding its operation. Firstly, the voltage deviates from its nominal value because droop control is realized by decreasing the DC output voltage level, a drop caused by the implementation of a virtual output impedance loop in the primary level. Moreover, although the implementation is easy and simple, the conventional droop method suffers from poor load sharing, especially when the line impedances are not negligible [3]. Due to the voltage drop across the line impedances, there is an output voltage mismatch among different converters which is needed for the natural power flow in dc systems but affects negatively the current sharing accuracy [4].

In order to overcome the limitations of the primary (droop) control, a secondary control scheme is implemented with the aim of achieving both voltage regulation and current sharing. This type of control can achieve global controllability of the MG as opposed to the primary control which is local and does not have intercommunications with other DG units [5]. Conventionally, a centralized secondary controller can be used, as presented in Figure 1. In this case, the DG units are locally controlled by a primary

☆This manuscript is submitted for the CES student conference organised by Department of Energy Technology, Aalborg University.
*Corresponding author:
Email addresses: imexis16@student.aau.dk (I. Mexis), hheo16@student.aau.dk (H. Heo)

and a secondary control that makes use of a remote sensing block in order to measure and send the needed parameters to the controller via a low-bandwidth communication system. The secondary controller compares the measured values with the references and sends the suitable output signal through the communications channel to each DG unit primary control. The disadvantage of this topology is the decreased reliability because the loss of a specific link can cause the failure of the respective unit resulting in overstressing of the other units, lead to overall loss of stability and cascaded failures [3].

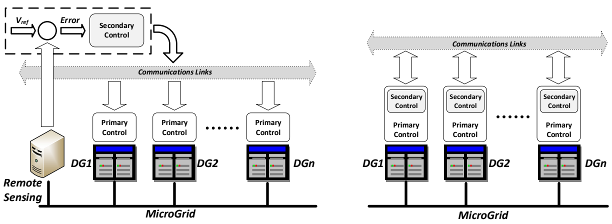

Figure 1: Centralized against distributed secondary control.

An alternative solution to the single centralized controller is the use of a distributed controller. This is implemented by using primary and secondary controllers together as a local controller in each DG unit. In this case, each secondary controller collects the voltage and current measurements of the other DG units, average them and sends the appropriate control signals to the primary level. Distributed control offers improved reliability, simpler communication network and easier scalability [3]. One of the most popular solutions that offers an autonomous operation and enhanced system performance is the containment and dynamic consensus–based distributed coordination control. This type of control can properly regulate the output voltage magnitudes into a prescribed range instead of only controlling the average voltage value and at the same time achieve accurate current sharing. Additionally, the system is improved in terms of reliability and robustness since each converter needs to exchange information only with its neighbours [6].

The sections of this paper are organized as follows. Section 2 shows the mathematical model extraction process for all the three types of controllers. Section 3 presents the tuning of the control parameters which is done based on the eigenvalue locus. In Section 4, a tradeoff analysis is presented with the aim of highlighting the tradeoffs within the secondary control. Section 5 demonstrates the results obtained for the different control schemes, according to the realized simulation tests in Matlab/Simulink. Finally, Section 6 summarizes the paper and gives the conclusions.

2. Mathematical model

In this section, the mathematical model of the DC microgrid is built in order to analyze the dynamic response performance of the droop and secondary control method.

2.1. Traditional secondary controller

The structure of the conventional secondary controller can be seen in Figure 2. It consists of a common PI controller for all four converters which provides the voltage correction term δV in order to control the average voltage to follow the reference. Moreover, there are four identical PI controllers, one for each converter, which provide the voltage correction term δV_i in order to equalize the current of the i^{th} converter to the average current.

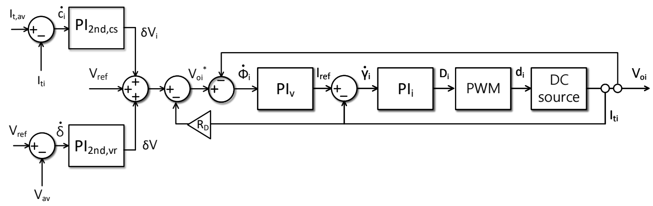

Figure 2: Scheme of the droop and traditional distributed secondary control for the i^{th} DG unit in a DC MG.

2.1.1. Mathematical model in state-space form including the traditional secondary control

The average-value modeling theory is applied in order to replace the discontinuous switching cells with continuous blocks that represent the averaged behavior of the switching cell within a prototypical switching interval [7]. Based on this theory, the state-space model for a typical structure of an islanded DC MG consisting of four parallel connected buck converters(Figure 3) is built. The converters are connected via three lines which are assumed to be purely resistive and they are supplied by four energy storage systems(ESS).

In the case under study it is assumed that all four converters are identical and they are supplied by equal DC sources, i.e. $L_i = L, R_{Li} = R_L, C_i = C, V_{dci} = V_{dc}$ for $i = 1$ to 4. Furthermore, they supply four resistive local loads. The converters have the same capability and it is desired to output the same amount of current. Therefore, in order to achieve the current sharing between them, i.e. $R_{Di} \cdot I_{ti} = R_{D(i+1)} \cdot I_{t(i+1)}$ for $i = 1$ to 3 , the same value of droop gain R_D has to be selected for each of them.

The control diagram of the i^{th} converter is presented in Figure 2, including the droop and the secondary controller whose task is to restore the nominal values of the voltages inside the MG and share the current proportionally.

Applying Kirchhoff's voltage and current laws in Figure 3, the following equations can be written for the

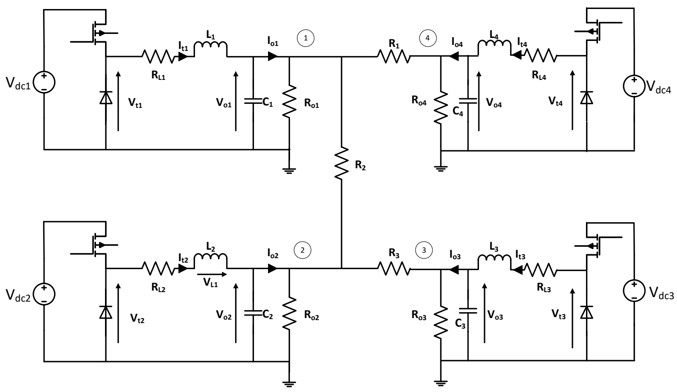

Figure 3: Electrical scheme of a DC ImG composed of four parallel connected converters with resistive loads.

i^{th} converter:

$$\frac{dV_{oi}}{dt} = \frac{1}{C} \cdot I_{ti} - \frac{1}{C} \cdot I_{oi} \tag{1}$$

$$\frac{dI_{ti}}{dt} = -\frac{1}{L} \cdot V_{oi} - \frac{R_L}{L} \cdot I_{ti} + \frac{1}{L} \cdot V_{ti} \tag{2}$$

According to the control diagram of Figure 2, the following equations can be written:

$$\frac{d\delta}{dt} = V_{ref} - V_{av} \tag{3}$$

$$\frac{dc_i}{dt} = I_{av} - I_i \tag{4}$$

$$\delta V = k_{ps} \cdot \frac{d\delta}{dt} + k_{is} \cdot \delta \tag{5}$$

$$\delta V_i = k_{ps2} \cdot \frac{dc_i}{dt} + k_{is2} \cdot c_i \tag{6}$$

$$\frac{d\Phi_i}{dt} = V_{ref} - V_{oi} - R_D \cdot I_{ti} + \delta V + \delta V_i \tag{7}$$

$$I_{refi} = k_{pv} \cdot \frac{d\Phi_i}{dt} + k_{iv} \cdot \Phi_i \tag{8}$$

$$\frac{d\gamma_i}{dt} = I_{refi} - I_{ti} \tag{9}$$

$$D_i = \frac{d\gamma_i}{dt} \cdot k_{pi} + k_{ii} \cdot \gamma_i \tag{10}$$

The output voltage of the buck converter is calculated as:

$$V_{ti} = D_i \cdot V_{dci} \tag{11}$$

The load current magnitudes I_{oi} contained in the voltage equations of the four converters(Equation 1) can be expressed in vector form as:

$$\hat{I}_o = L \cdot \hat{V}_o + \frac{\hat{V}_o}{\hat{R}_o} \tag{12}$$

where L is a conductance matrix, calculated in Appendix A. By substituting the expression for the load current into Equation 1 and manipulating Equations 1–11, the mathematical model can be obtained. This model can be written in state-space form as follows:

$$\begin{aligned} \frac{dx}{dt} &= A \cdot x + B \cdot u \\ y &= C \cdot x + D \cdot u \end{aligned} \tag{13}$$

where:

- $x = [V_{o1}, I_{t1}, \Phi_1, \gamma_1, c_1, V_{o2}, I_{t2}, \Phi_2, \gamma_2, c_2, V_{o3}, I_{t3}, \Phi_3, \gamma_3, c_3, V_{o4}, I_{t4}, \Phi_4, \gamma_4, c_4, \delta]$
- $y = [V_{o1}, I_{t1}, V_{o2}, I_{t2}, V_{o3}, I_{t3}, V_{o4}, I_{t4}]$
- $u = V_{ref}$
- A: 21x21 system matrix
- B: 21x1 input matrix
- C: 8x21 ouput identity matrix
- D: 8x1 zero feedforward matrix

After having extracted the mathematical model, its accuracy is tested by comparing it with the Simulink model. The results can be seen in Figure 4, where the converter output voltages and currents are presented. Both primary and secondary control are activated from the beginning. By observation of Figure 4, it can be concluded that the mathematical model matches very accurately the Simulink one. Thus, it can be used for the tuning of the PI control parameters.

2.2. Consensus based controller

Systems that employ the previous approach, i.e. consist of a fully connected communication network, are susceptible to failure. If one link fails, the whole control functionality is impaired. Besides, the future extension can also be a challenging issue [3]. Instead, the distributed consensus-based controller concept can be used, whose control diagram is given in Figure 6. In this case, each converter transmits a set of data to its neighbours, Ψ_i=[$\overline{v_i}$, i_i^{pu}], where $\overline{v_i}$ and i_i^{pu} are the estimated voltage across the MG and the pu current of the i^{th} converter(Figure 5). Thus, the communication network is sparse and does not require a high level of connectivity.

As can be seen in Figure 6, the controller consists of a voltage regulator and a current regulator. The former consists of a voltage observer and a PI controller H_i. The voltage observer of the i^{th} converter estimates

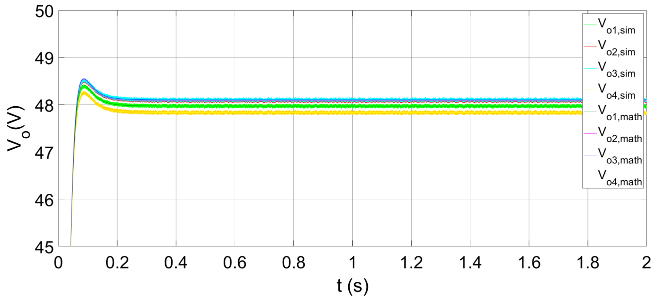

(a)

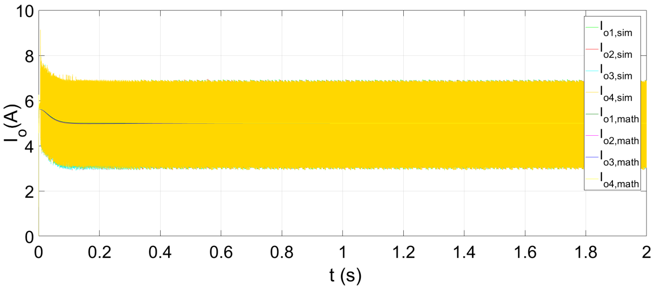

(b)

Figure 4: Comparison between the mathematical and Simulink model when the MG is operated under the traditional secondary control. (a) converter output voltages. (b) converter output currents.

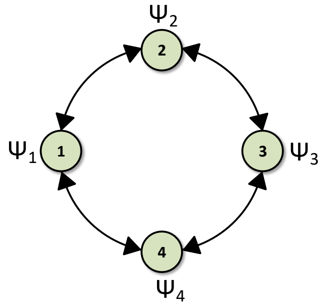

Figure 5: Communication network between the four converters.

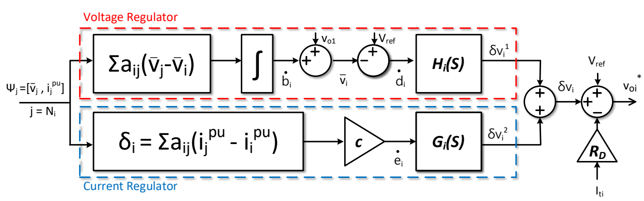

Figure 6: Distributed consensus controller of the i^{th} converter.

the averaged voltage $\overline{v_i}$ across the microgrid which is compared to the reference voltage v_{ref} and produces the voltage correction term δv_i^1. The estimated voltage is calculated by processing the local voltage measurement and the neighbors' estimates. The communication weights a_{ij} obtain positive value when there is communication between the i_{th} and the j_{th} converter, otherwise they are equal to zero.

Regarding the proportional current sharing, it cannot be achieved by the droop mechanism due to the presence of the line impedances. Therefore, a current regulator is used. It consists of a PI controller G_i and the block δ_i which compares the local pu current with a weighted averaged of the neighbors' pu currents, producing the voltage correction term δv_i^2. The constant c is the coupling gain between the voltage and current regulators.

2.2.1. Mathematical model in state-space form including the consensus–based secondary control

In order to extract the mathematical model of the consensus–based controller, the equations used are similar to the case of the traditional one, therefore they are omitted here. The main modification is done in the voltage correction terms. More specifically, three new variables are introduced, i.e. $\frac{db_i}{dt}$, $\frac{dd_i}{dt}$ and $\frac{de_i}{dt}$ for the i^{th} converter, as can be seen in Figure 6. Again, by manipulating the equations, the mathematical model can be extracted and written in state-space form as follows:

$$\begin{aligned} \frac{dx}{dt} &= A_c \cdot x + B_c \cdot u \\ y &= C_c \cdot x + D_c \cdot u \end{aligned} \tag{14}$$

where:

- $x = [V_{o1}, I_{t1}, \Phi_1, \gamma_1, b_1, d_1, e_1, V_{o2}, I_{t2}, \Phi_2, \gamma_2, b_2, d_2, e_2, V_{o3}, I_{t3}, \Phi_3, \gamma_3, c_3, b_3, d_3, e_3, V_{o4}, I_{t4}, \Phi_4, \gamma_4, b_4, d_4, e_4]$
- $y = [V_{o1}, I_{t1}, V_{o2}, I_{t2}, V_{o3}, V_{o4}, I_{t4}]$
- $u = V_{ref}$
- A_c: 28x28 system matrix
- B_c: 28x1 input matrix
- C_c: 8x28 ouput identity matrix
- D_c: 8x1 zero feedforward matrix

Figure 7 provides a comparison between the Simulink and mathematical model. It can be observed that there is an accurate matching between the two models after 0.18s. Thus, the obtained mathematical model can be used for the tuning of the PI parameters.

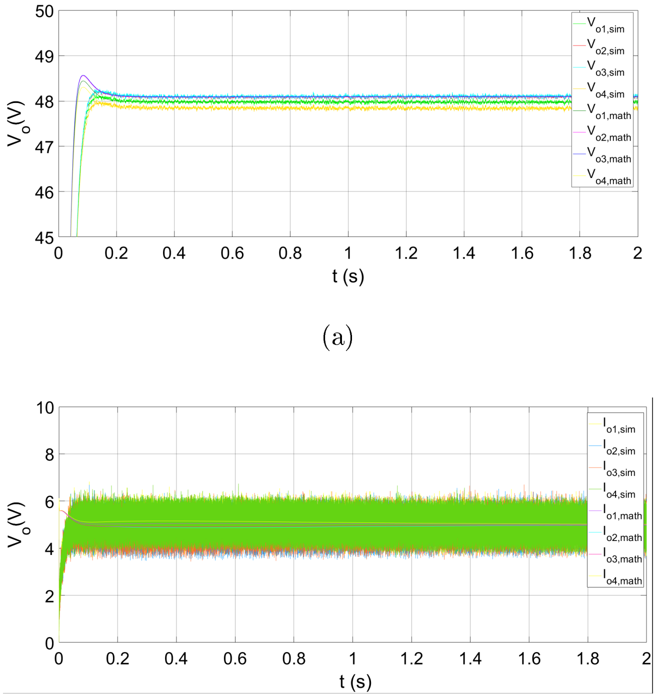

Figure 7: Comparison between the mathematical and Simulink model when the MG is operated under the consensus–based secondary control. (a) converter output voltages. (b) converter output currents.

2.3. Containment and consensus–based controller

As it was mentioned above, there is a need for a control strategy which bounds the voltage magnitudes within a prescribed range. This can be achieved by applying the containment–based voltage controller. At the same time, in order to ensure accurate proportional current sharing among the DG units, the dynamic current consensus–based control is implemented. Therefore, the coordination of these two controllers achieves both control objectives. Essentially, this control scheme can achieve to control all the bus voltages and not only the average value of them, which is the case with most of the algorithms found in the literature [5], [8], [9].

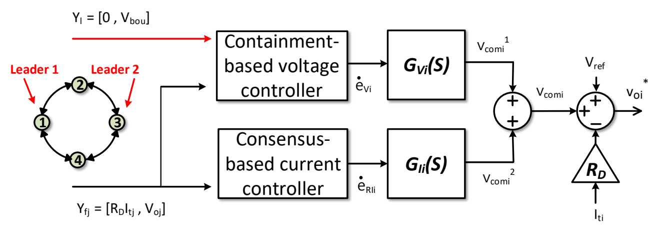

Figure 8: Configuration of the Containment and Consensus-based Distributed Coordination Controller in a DC MG.

The configuration of this controller can be seen in Figure 8 and it is explained briefly. The correction item $\frac{de_{Vi}}{dt}$ is generated for the i^{th} converter in order to bound all the bus voltages within a reasonable range, i.e. between the lower bound $v_{L,bou}$ and the upper bound v_{Ubou}. The definition of the controller is given next:

$$\frac{de_{Vi}}{dt} = \sum_{j\in N_i} a_{ij}\cdot(v_j - v_i) + \sum_{l\in R_i} b_{il}\cdot(v_{bou} - v_i) \qquad (15)$$

where N_i the set of the i^{th} controller neighbours chosen from followers(controllers that receive information from their neigbours), R_i the set of leaders(controllers that only provide information to their neigbours), v_{bou} the voltage boundary reference (either $v_{u,bou}$ or $v_{L,bou}$).

This type of controller is more suitable for systems with relatively large line impedances and high current sharing requirements. In addition, it provides high degree of freedom, since it can either satisfy the bus voltage bound requirement through setting error saturation of current sharing performance or focus on achieving accurate current sharing by enlarging the voltage boundary [6].

Regarding the consensus-based current controller, it generates the correction item $\frac{de_{RIi}}{dt}$ with the aim of achieving accurate current sharing, which equals to:

$$\frac{de_{RIi}}{dt} = \sum_{j\in N_i} a_{ij}\cdot(R_{Dj}\cdot I_{tj} - R_{Di}\cdot I_{ti}) \qquad (16)$$

Moreover, $Y_{fj} = [R_{Dj}\cdot I_{tj}, V_{oj}]$ and $Y_l = [0, V_{bou}]$ are the information format from the followers and leaders respectively [10].

2.3.1. Mathematical model in state-space form including the containment and consensus–based secondary control

Similarly to the previous cases, the mathematical model of the containment and consensus–based controller is derived. In this case, two new variables are introduced, i.e. $\frac{de_{Vi}}{dt}$, $\frac{de_{RIi}}{dt}$ for the i^{th} converter, according to Figure 8. The mathematical model represented in state-space form is given below:

$$\begin{aligned} \frac{dx}{dt} &= A_{ct}\cdot x + B_{ct}\cdot u \\ y &= C_{ct}\cdot x + D_{ct}\cdot u \end{aligned} \qquad (17)$$

where:

- $x = [V_{o1}, I_{t1}, \Phi_1, \gamma_1, e_{V1}, e_{RI1}, V_{o2}, I_{t2}, \Phi_2, \gamma_2, e_{V2}, e_{RI2}, V_{o3}, I_{t3}, \Phi_3, \gamma_3, e_{V3}, e_{RI3}, V_{o4}, I_{t4}, \Phi_4, \gamma_4, e_{V4}, e_{RI4}]$

- $y = [V_{o1}, I_{t1}, V_{o2}, I_{t2}, V_{o3}, V_{o4}, I_{t4}]$

- $u = [V_{ref}, Vu, Vl]$

- A_{ct}: 24x24 system matrix
- B_{ct}: 24x1 input matrix
- C_{ct}: 8x24 ouput identity matrix
- D_{ct}: 8x3 zero feedforward matrix

Based on Figure 9, it can be concluded that the mathematical model matches the Simulink accurately and thus it can be utilized for the tuning of the control parameters.

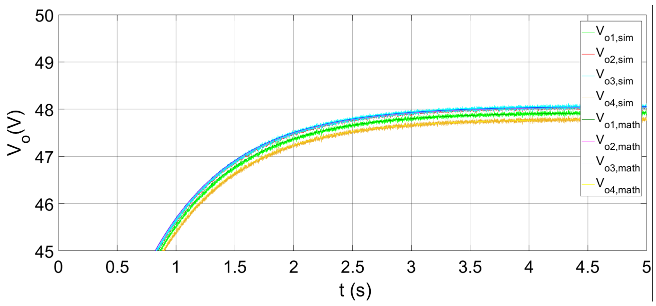

(a)

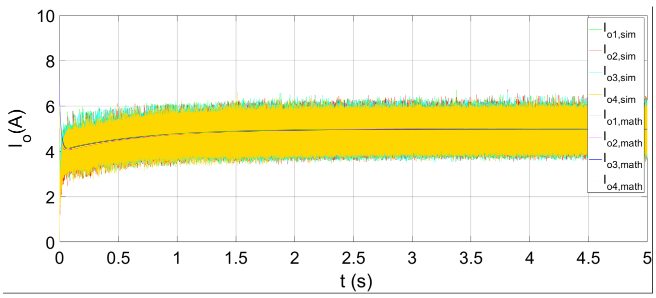

(b)

Figure 9: Comparison between the mathematical and Simulink model when the MG is operated under the containment and consensus–based secondary control. (a) converter output voltages. (b) converter output currents.

3. Eigenvalue analysis

3.1. Tuning of the control parameters in case of the traditional secondary control implementation

Based on the mathematical model, the eigenvalue locus method can be used to analyze the dynamic response of the system. The roots of the characteristic equation of the system's state matrix are the eigenvalues of matrix A. Therefore, by plotting the latter for varying PI gain values, the stability and the dynamic response of the system can be examined and thus the appropriate gain values can be determined. Totally, eight PI parameters have to be tuned for each converter, i.e. the gains for the primary loop current and voltage PIs as well as those of the secondary control PIs.

Initially, the current loop parameters are tuned. Keeping the other parameters fixed at 0.1 and varying the integral gain k_{ii} from 110 to 300, the eigenvalue shifting trajectories are shown in Figure 10. It can be concluded that by increasing the integral terms, the current fluctuations during dynamical process are enlarged but the errors are eliminated more rapidly. Therefore, a middle value is chosen in order to avoid high frequency oscillations as well as make the system faster. The chosen value for the integral term of the current PI controller is $k_{ii} = 165$.

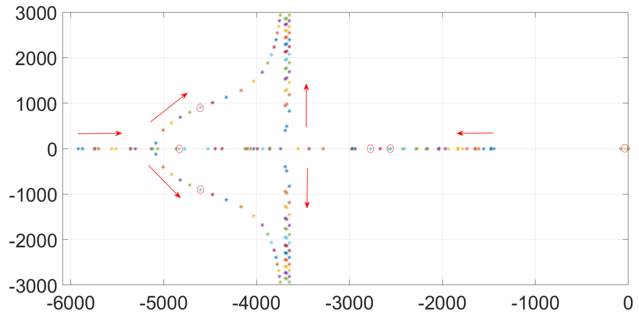

Figure 10: Eigenvalue locus plot with k_{ii} varying.

Following the same procedure, the rest of the gain values of the current and voltage PI controllers are determined. Then, the secondary gains are chosen. In Figure 11 (a), the eigenvalue shifting trajectories for variation of the proportional gain of the voltage PI secondary control k_{ps} from 0.05 to 0.17 are presented. It can be observed that by increasing k_{ps}, the system becomes more damped. In this case $k_{ps} = 0.05$ is chosen. Regarding the integral gain k_{is}, its increase leads to a more damped and faster system(Figure 11 (b)). Figure 12 presents the eigenvalue shifting trajectories for variation of the current sharing block PI gains.

Finally, the robustness of the controller is tested by gradually increasing the resistive loads from their current values(Table 1) to 1000. From Figure 13 it can be seen that the eigenvalues do not change significantly, meaning that the controller has a robust and stable performance during a wide range of loads. This indicates that the control scheme does not require prior knowledge of the load information in the system.

The chosen values of the PI gains as well as the rest of the system parameters are given in Table 1. Moreover, Table 2 summarizes the effect of the control parameters on the dynamic response of the system.

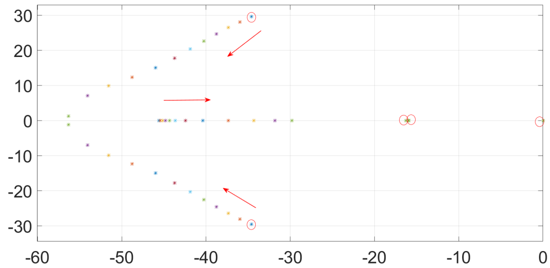

(a)

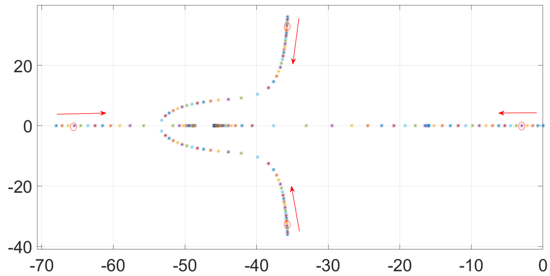

(b)

Figure 11: Eigenvalue locus plot with k_{ps} and k_{is} varying

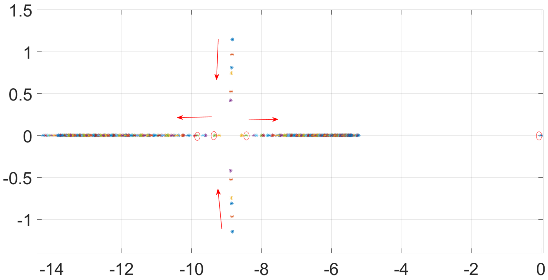

(a)

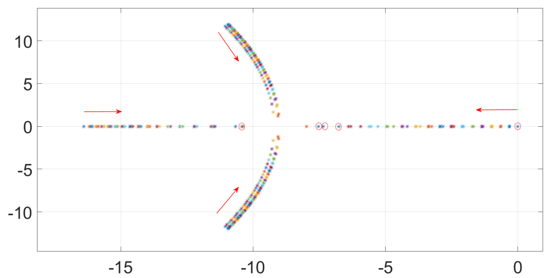

(b)

Figure 12: Eigenvalue locus plot with k_{ps2} and k_{is2} varying

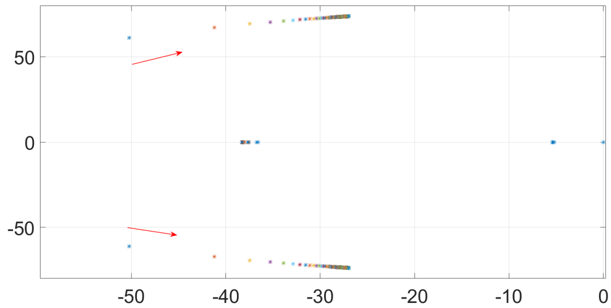

Figure 13: Eigenvalue locus plot with the resistive load values increasing from their current values to 1000, with the MG controlled under traditional secondary control

Table 1: DC MG control-system parameters

Parameters	**Symbol**	**Value**
DC power supply	V_{dc}	100 V
Converter inductance	L	1.8 mH
Inductor resistance	R_L	0.2 Ω
Converter capacitance	C	2.2 mF
Line 1 resistance	R_1	0.03 Ω
Line 2 resistance	R_2	0.06 Ω
Line 3 resistance	R_3	0.09 Ω
Resistive load 1	R_{o1}	20 Ω
Resistive load 2	R_{o2}	15 Ω
Resistive load 3	R_{o3}	10 Ω
Resistive load 4	R_{o4}	5 Ω
Droop gain	R_D	3 Ω
Primary control gains	**Symbol**	**Value**
Voltage proportional term	k_{pv}	0.17
Voltage integral term	k_{iv}	9
Current proportional term	k_{pi}	0.1
Current integral term	k_{ii}	165
Traditional secondary control gains	**Symbol**	**Value**
Voltage proportional term	k_{ps}	0.05
Voltage integral term	k_{is}	20
Current proportional term	k_{ps2}	0.05
Current integral term	k_{is2}	15

Table 2: Stability analysis conclusion

Control parameters	**Response speed**	**Damping**
k_{ps} ↑	↓	↑
k_{is} ↑	↑	↑
k_{ps2} ↑	↓	↑
k_{is2} ↑	↑	↑

3.2. Tuning of the control parameters in case of the consensus–based secondary control implementation

Similar to the case of the traditional secondary control, the eigenvalue method was used in order to tune the PI control parameters. Their values are given in Table 3.

It is worth mentioning that also in this case, the control was tested and it was robust in the whole load range.

Table 3: System control parameters when the consensus based controller is applied

Primary control gains	Symbol	Value
Voltage proportional term	k_{pvc}	0.17
Voltage integral term	k_{ivc}	8
Current proportional term	k_{pic}	0.1
Current integral term	k_{iic}	120
Consensus based secondary control gains	**Symbol**	**Value**
Voltage proportional term	k_{psc}	0.1
Voltage integral term	k_{isc}	9
Current proportional term	k_{ps2c}	0.04
Current integral term	k_{is2c}	4

3.3. Tuning of the control parameters in case of the containment and consensus–based secondary control implementation

Finally, for the coordination controller, the chosen gains are provided in Table 4. Similar to the two aforementioned cases, the eigenvalues are not affected significantly by the load change, proving the robustness of the designed controller.

Table 4: System control parameters when the containment and consensus–based controller is applied

Primary control gains	Symbol	Value
Voltage proportional term	$k_{pv,cont}$	0.17
Voltage integral term	$k_{iv,cont}$	8
Current proportional term	$k_{pi,cont}$	0.09
Current integral term	$k_{ii,cont}$	130
Containment and consensus–based secondary control gains	**Symbol**	**Value**
Voltage proportional term	$k_{ps,cont}$	0.2
Voltage integral term	$k_{is,cont}$	4
Current proportional term	$k_{ps2,cont}$	0.17
Current integral term	$k_{is2,cont}$	30

4. Tradeoff analysis between current sharing and voltage magnitude regulation

In this chapter, the tradeoff between current sharing and voltage magnitude regulation within the traditional secondary control level is analyzed. The simplified structure of an islanded MG is shown in Figure 14, which presents a typical islanded MG with four DGs supplying four local loads. The converters are connected through different line impedances and they are supplied by equal DC sources. In the following, the necessary equations are derived according to the control diagram and the circuit topology in order to perform the tradeoff analysis. When the DG units are operated under droop control, their voltages are given by Equation 18:

$$V_{oi} = V_{ref} - R_D \cdot I_{ti} \tag{18}$$

By activating only the voltage regulation block of Figure 2, they are modified as shown below:

$$V_{oi} = V_{ref} - R_D \cdot I_{ti} + \delta V \tag{19}$$

By applying only the current regulation block, they are modified based on Equation 20:

$$V_{oi} = V_{ref} - R_D \cdot I_{ti} + \delta V_i \tag{20}$$

where V_{oi} and I_{ti} are the output voltage and current of the i^{th} converter respectively, for $i = 1 - 4$.

Furthermore, according to Figure 3, the node equations can be written for each of the four nodes. In order to obtain a relationship between the output voltage and current of the i^{th} converter, the output voltages of the other three converters are assumed to be equal to the average voltage. Thus, four equations are extracted:

$$V_{o1} = \frac{1}{\frac{1}{R_{o1}} + \frac{1}{R_1} + \frac{1}{R_2}} \cdot I_{t1} + \frac{\frac{1}{R_1} + \frac{1}{R_2}}{\frac{1}{R_{o1}} + \frac{1}{R_1} + \frac{1}{R_2}} \cdot V_{ave} \tag{21}$$

$$V_{o2} = \frac{1}{\frac{1}{R_{o2}} + \frac{1}{R_2} + \frac{1}{R_3}} \cdot I_{t2} + \frac{\frac{1}{R_2} + \frac{1}{R_3}}{\frac{1}{R_{o2}} + \frac{1}{R_2} + \frac{1}{R_3}} \cdot V_{ave} \tag{22}$$

$$V_{o3} = \frac{1}{\frac{1}{R_{o3}} + \frac{1}{R_3}} \cdot I_{t3} + \frac{\frac{1}{R_3}}{\frac{1}{R_{o3}} + \frac{1}{R_3}} \cdot V_{ave} \tag{23}$$

$$V_{o4} = \frac{1}{\frac{1}{R_{o4}} + \frac{1}{R_1}} \cdot I_{t4} + \frac{\frac{1}{R_1}}{\frac{1}{R_{o4}} + \frac{1}{R_1}} \cdot V_{ave} \tag{24}$$

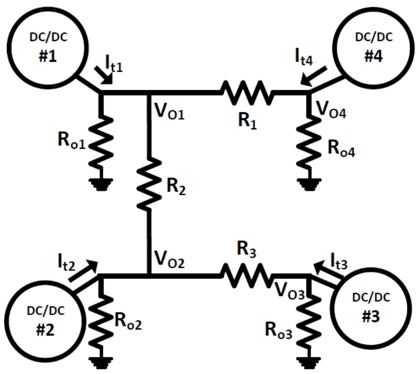

Figure 14: The simplified structure of an islanded MG.

The graphical analysis can be done with the set of Equations 18-24. Next, in the first two cases, the voltage regulation block of the secondary controller of Figure 2 is activated, i.e. the focus is put on voltage magnitude regulation. In case 3, the current regulation block of the secondary controller of Figure 2 is activated, i.e. the focus is put on current sharing regulation.

4.1. Focus on voltage magnitude regulation

In the first case $R_D = 0.3\,\Omega$ and the line resistances are equal to $R_1 = 0.3\,\Omega$, $R_2 = 0.6\,\Omega$ and $R_3 = 0.9\,\Omega$. According to Figure 15, it can be seen that the voltage restoration control makes the error of current sharing even wider. Even though the deviation of voltage magnitudes

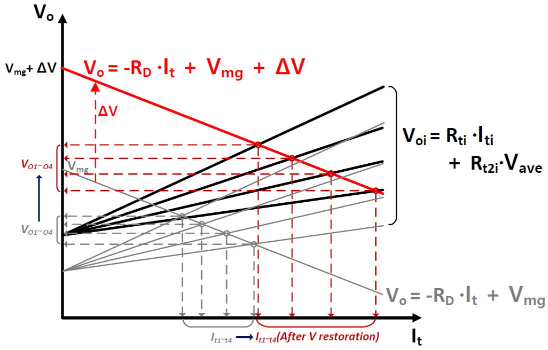

Figure 15: Voltage magnitude restoration control for four parallel DGs with small droop gain and large line resistances.

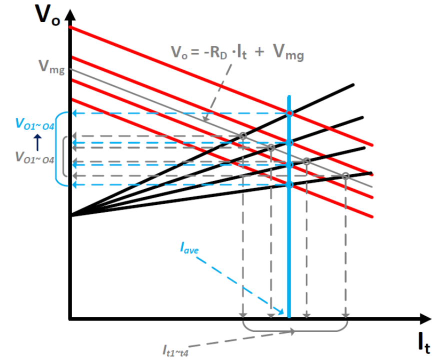

Figure 17: Current sharing regulation control for four parallel DGs with small droop gain and large line resistances.

from nominal value is small due to the voltage restoration control, current sharing cannot be achieved.

In the second case $R_D = 3\,\Omega$ and the lines resistances are equal to $R_1 = 0.03\,\Omega$, $R_2 = 0.06\,\Omega$ and $R_3 = 0.09\,\Omega$. According to Figure 16 it can be seen that more accurate current sharing can be achieved compared to the first case due to the presence of big droop gain. The values of the converter output voltages are very close to the nominal value.

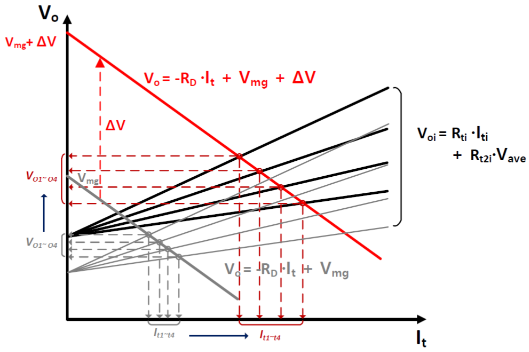

Figure 16: Voltage magnitude restoration control for four parallel DGs with large droop gain and small line resistances.

4.2. Focus on current sharing

In this case $R_D = 0.3\,\Omega$ and $R_1 = 0.3\,\Omega$, $R_2 = 0.6\,\Omega$, $R_3 = 0.9\,\Omega$. From Fig 17 it can be seen that this control strategy makes the output currents of the four converters equal, i.e the current sharing is achieved accurately but there is no voltage restoration. In case of large droop gain and small line resistances, the results are almost the same, i.e. accurate current sharing is achieved but the voltages do not change significantly, so the corresponding Figure is omitted.

Based on the above analysis, it can be concluded that the current sharing regulation has less tradeoff effects on the deviation of voltage magnitudes than the tradeoff effect of voltage magnitude restoration on the deviation of current sharing. In other words, the regulation of the voltage magnitudes to their nominal values causes large deviation in the current sharing. On the contrary, the current sharing regulation has a small effect on the voltage magnitude deviation. Therefore, in order to solve the tradeoff within the secondary control, the best solution is to apply a control strategy which achieves accurate current sharing and controls the voltage magnitudes within a certain band instead of controlling the average value of voltage magnitudes being constant [6].

5. Simulations

Within this section, a number of simulations is implemented to test the system response under different operating conditions, i.e. in steady state, under load changes and fault conditions.

5.1. Droop control

In this subsection, the effect of both the droop gain R_D and line resistances is analyzed through a number of indicative simulations. In Figure 18 the converter output currents and voltages are presented. The droop control is activated at $t_p = 1s$. As can be seen, by choosing a large value for the droop gain($R_D = 3$), the current sharing is achieved but its negative effect on the DC output voltages is obvious, since they present a big deviation from their nominal values, i.e 48V. On the other hand, the choice of a smaller droop gain would lead to the decrease of voltage deviation but at the same time the desired current sharing cannot be achieved accurately.

Moreover, by comparing Figures 18 and 19, it can be concluded that the increase in the absolute values of lines resistances as well as in the difference between them deteriorates the current sharing accuracy.

The tradeoff effect of the droop gain on the voltage regulation and current sharing is obvious. Therefore, to achieve both control objectives, the secondary level is applied, the results of which are presented in the next subsection.

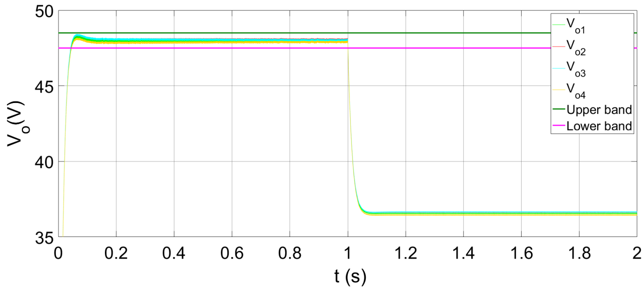

(a)

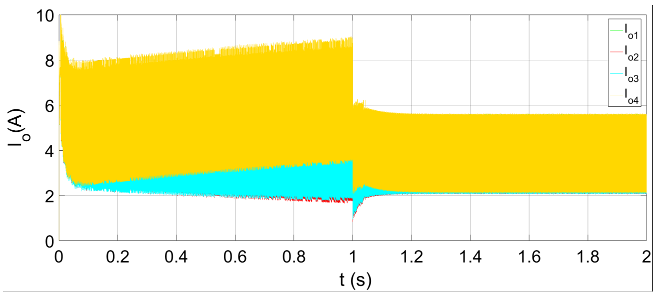

(b)

Figure 18: Converter outputs with droop control activated at $t_p = 1s$ and $R_1 = 0.03, R_2 = 0.06, R_3 = 0.09$. (a) output voltages. (b) output currents.

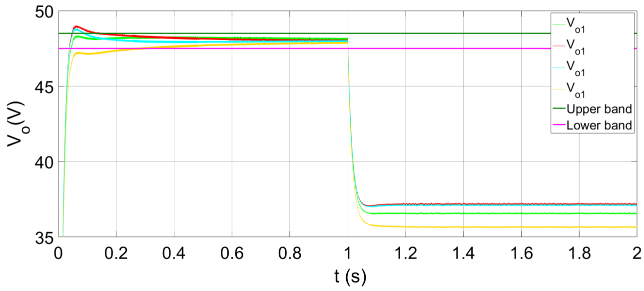

(a)

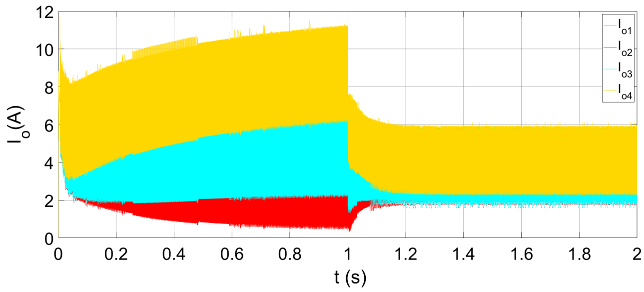

(b)

Figure 19: Converter outputs with droop control activated at $t_p = 1s$ and $R_1 = 0.3, R_2 = 0.6, R_3 = 0.9$. (a) output voltages. (b) output currents.

5.2. Traditional secondary control

In the first scenario, only the voltage regulation block is activated. Droop control is activated at $t_p = 0s$, whereas secondary control is activated at $t_s = 0.5s$. By obervation of Figure 20, it can be seen that the voltage restores and stays within the allowed band and at the same time the current sharing is very accurate due to the presence of the big droop gain. On the contrary, when the droop gain is decreased and the line resistances are increased, the output voltage of converter 4 cannot stay within the band and the current sharing is not achieved, as Figure 21 depicts.

In the second scenario, only the current regulation block is activated with the aim of presenting its effects on voltage regulation and current sharing. As can be clearly observed in Figure 22, the current sharing is accurate but in this case no voltage restoration is provided. For small droop gain value and larger line resistances, the results are almost the same, thus they are not presented here.

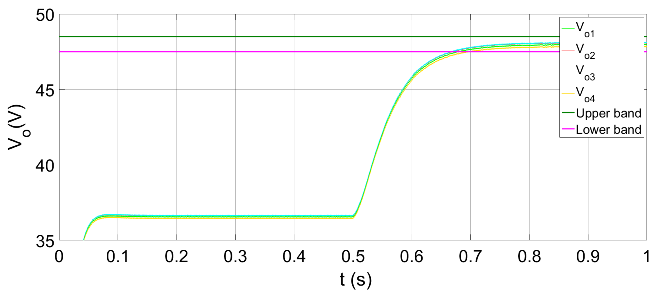

(a)

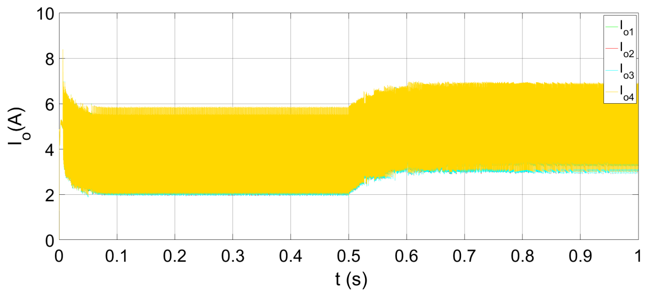

(b)

Figure 20: Converter outputs with focus on voltage magnitude regulation for large droop gain and small line resistance values. (a) output voltages. (b) output currents.

As it was concluded in the Tradeoff analysis section, when the voltage magnitudes are regulated to their nominal values, significant deviations are observed in the current sharing. This conclusion can be verified by Figures 20, 21. On the other hand, the current sharing regulation has a small impact on the voltage magnitude deviation (comparing the case of big R_D and small line resistances with the case of small R_D and big line resistances, the voltage magnitudes are almost the same).

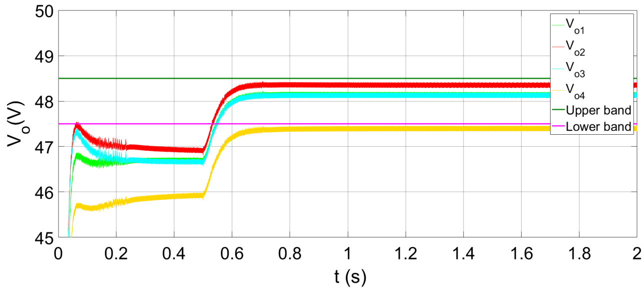

(a)

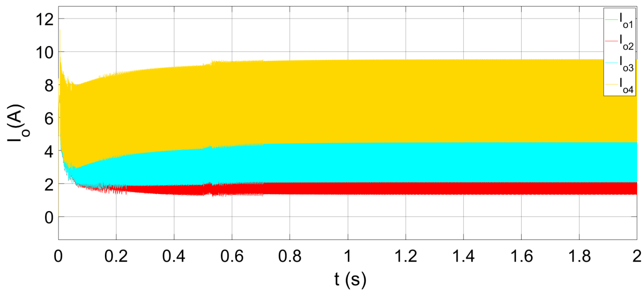

(b)

Figure 21: Converter outputs with focus on voltage magnitude regulation for small droop gain and large line resistance values. (a) output voltages. (b) output currents.

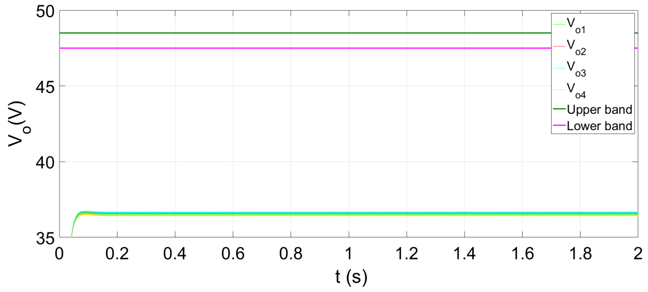

(a)

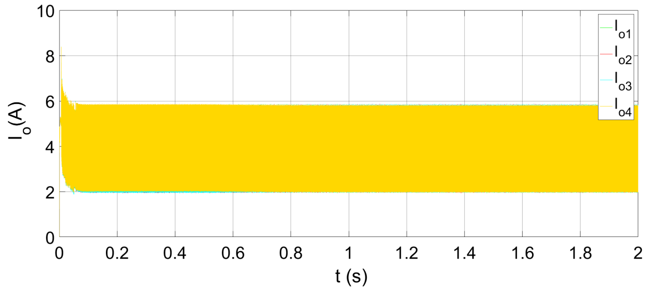

(b)

Figure 22: Converter outputs with focus on current sharing regulation for large droop gain and small line resistance values. (a) output voltages. (b) output currents.

Finally, both blocks are activated at $t_s = 0.5s$ and during the simulation a load change happens at $t_l = 1s$, i.e. the resistance values are changed to $R_{o1} = 21\Omega$, $R_{o2} = 16\Omega$, $R_{o3} = 9\Omega$, $R_{o4} = 4\Omega$. It can be seen that both control objectives are achieved and at the same time the secondary contoller restores the voltage drop within 0.15s after the load change(Figure 23).

5.3. Consensus-based control

To end up with a more reliable system, the consensus-based control is implemented and the results can be seen in the following figures. In Figure 24, the secondary control is activated at $t_s = 0.5s$ and after 0.5s a load change occurs. It can be observed that the control restores the DC voltages within 0.15s and all of them converge to 48V. In addition, the current is shared equally among all four converters.

Finally, in order to test the reliability of this type of controller, a communication failure is introduced between converters 1 and 2 at $t_f = 1s$, as Figure 25 depicts. It can be observed that the system continues working properly even after the failure, with the control objectives being fulfilled.

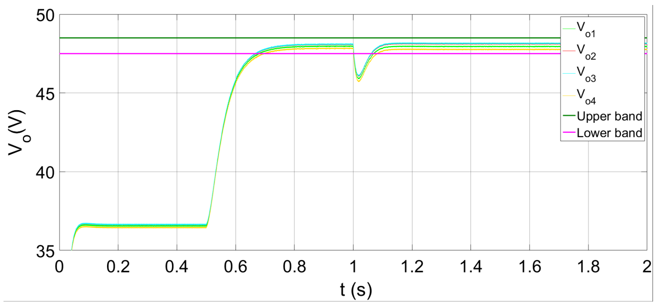

(a)

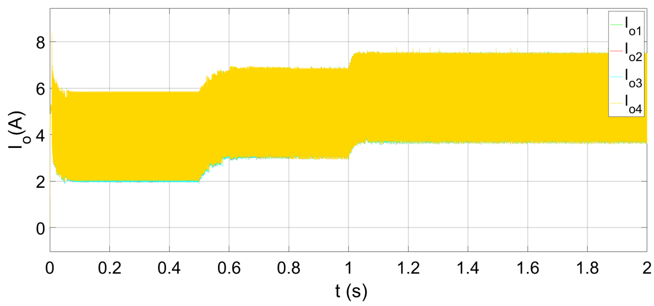

(b)

Figure 23: Performance of converter outputs under load change when the traditional secondary control is applied. (a) output voltages. (b) output currents.

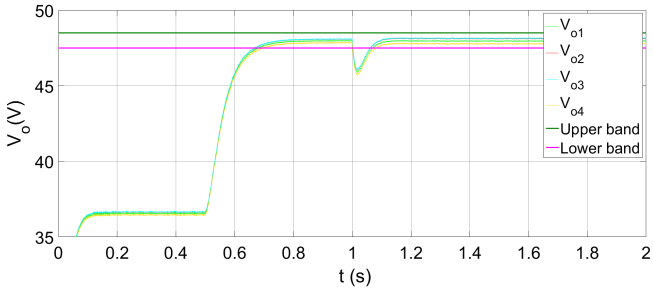

(a)

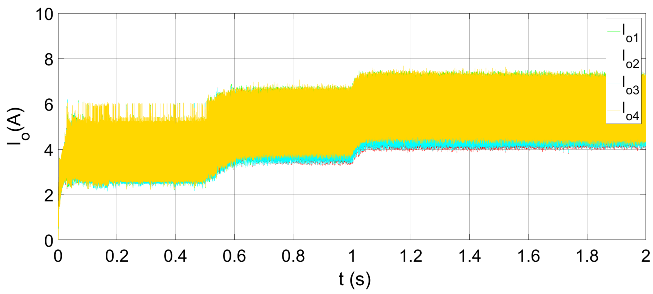

(b)

Figure 24: Performance of converter outputs under load change when the consensus secondary control is applied. (a) output voltages. (b) output currents.

5.4. Containment and consensus-based control

Finally, the system is operated under the containment and consensus-based control. In the simulation scenario of Figure 26, the voltage band is modified from [45.5, 50.5] to [40.5, 45.5] at $t_1 = 2s$ and changed back to [45.5, 50.5] at $t_3 = 4s$. In addition, a load change occurs at $t_2 = 3s$. As can be seen, the voltage magnitudes can follow the band change and stay within the limits, whereas the current sharing among the converters is not affected.

Then, the resiliency to a single communication link failure is studied. The communication between converters 1 and 2 is lost at $t_1 = 3s$. This situation is simulated and presented in Figure 27. It can be seen that the voltages stay within the band and the current sharing performance remains good. After that, the load is switched at $t_2 = 4s$ and it is shown that there is no impact on the performance. Therefore, it is concluded that since the communication network remains connected from the perspective of graph theory, the controller keeps robust performance during the steady-state and the transient operation.

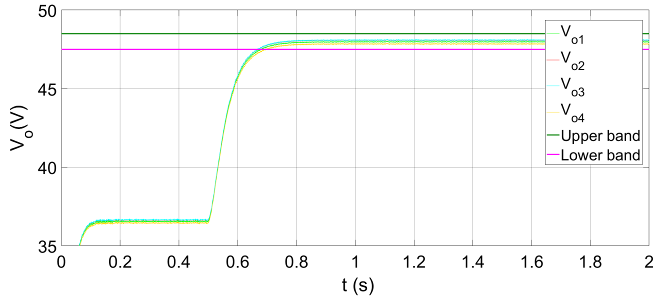

(a)

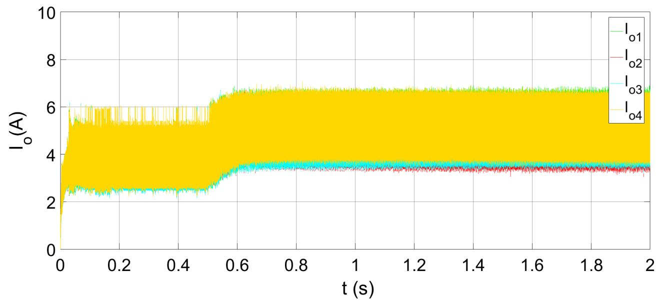

(b)

Figure 25: Converter outputs when the communication between converters 1 and 2 fails. (a) output voltages. (b) output currents.

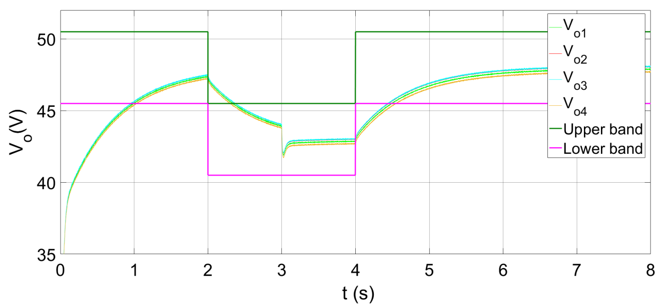

(a)

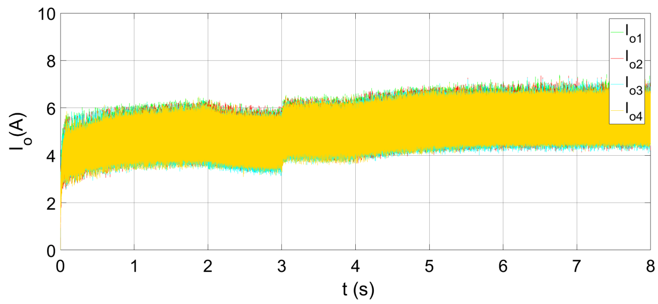

(b)

Figure 26: Performance assesment of voltage and current regulation during operation with varying voltage band and load change. (a) output voltages. (b) output currents.

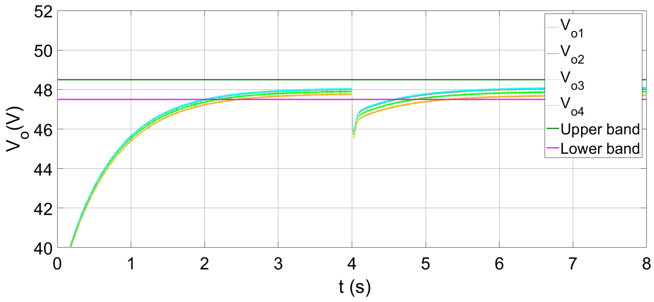

(a)

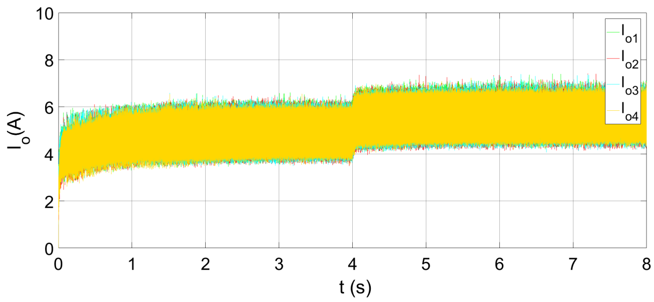

(b)

Figure 27: Performance assessment of voltage and current regulation under single communication failure and load change. (a) output voltages. (b) output currents.

6. Conclusion

This paper presents the first two levels of the three-level hierarchical control applied to an islanded DC MG. The primary control concept implemented by an addition of a virtual output resistance was proved to achieve the current sharing by regulating the droop gain. Nevertheless, the disadvantages of the voltage deviation from the nominal value and the presence of the line impedances which deteriorate the current sharing capability make imperative the use of a secondary control level. The traditional version of this controller was studied and a tradeoff analysis between the current sharing and the voltage magnitude regulation was made within this control level, leading to the conclusion that a control strategy which bounds the voltages into a prescribed range and achieves the proportional current sharing is needed. Initially, the consensus–based control was applied, a concept which uses a sparse communication network. Studies showed that it can achieve both control objectives and at the same time it presents resiliency to communication failure and increases the overall system reliability. Furthermore, to make it possible to bound the voltage magnitudes within a certain band and not just control their average value, the containment and consensus–based control concept was considered, presenting high performance during steady–state and dynamic operation.

Appendix A : Line conductance matrix

The line conductance matrix of Equation 12 is defined as:

$$L = B^T \cdot W \cdot B \tag{A.1}$$

where W is a diagonal matrix with size lxl(l the number of lines) in which the elements of the main diagonal contain the line conductance values. For the number of lines $l = n - 1$, where n the number of converters. In the case under study four converters are connected via three lines. Therefore W is given below:

$$W = \begin{bmatrix} \frac{1}{R_1} & 0 & 0 \\ 0 & \frac{1}{R_2} & 0 \\ 0 & 0 & \frac{1}{R_3} \end{bmatrix} \tag{A.2}$$

Regarding matrix B, its dimensions are lxn. In order to calculate the values of its elements, the current direction has to be defined first, as can be seen in Figure A.28:

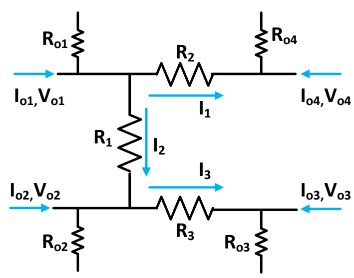

Figure A.28: Line and load topology for obtaining the relationship between the output currents and voltages.

As can be seen, line 1 connects converters 1 and 4 and I_1 flows from converter 1 to 4. Therefore $B_{11} = -1$ and $B_{14} = 1$. Converters 2 and 3 are not connected to line 1, so the corresponding elements $B_{12} = B_{13} = 0$. Following the same logic, the rest of the elements are calculated. Matrix B is given below:

$$B = \begin{bmatrix} -1 & 0 & 0 & 1 \\ -1 & 1 & 0 & 0 \\ 0 & -1 & 1 & 0 \end{bmatrix} \tag{A.3}$$

Substituting matrixes W and B into Equation A.1, matrix L is obtained. From Equation 12 the relationship between the load currents and the voltages can be found:

$$\begin{bmatrix} I_{o1} \\ I_{o2} \\ I_{o3} \\ I_{o4} \end{bmatrix} = \begin{bmatrix} \frac{1}{R_1} + \frac{1}{R_2} + \frac{1}{R_{o1}} & -\frac{1}{R_2} & 0 & -\frac{1}{R_1} \\ -\frac{1}{R_2} & \frac{1}{R_2} + \frac{1}{R_3} + \frac{1}{R_{o2}} & -\frac{1}{R_3} & 0 \\ 0 & -\frac{1}{R_3} & \frac{1}{R_3} + \frac{1}{R_{o3}} & 0 \\ -\frac{1}{R_1} & 0 & 0 & \frac{1}{R_1} + \frac{1}{R_{o4}} \end{bmatrix} \cdot \begin{bmatrix} V_{o1} \\ V_{o2} \\ V_{o3} \\ V_{o4} \end{bmatrix} \tag{A.4}$$

References

[1] R. Han, L. Meng, J. M. Guerrero, and J. C. Vasquez, “Distributed nonlinear control with event-triggered communication

to achieve current-sharing and voltage regulation in dc microgrids," *IEEE Transactions on Power Electronics*, vol. PP, no. 99, pp. 1–1, 2017.

[2] J. M. Guerrero, J. C. Vasquez, J. Matas, L. G. de Vicuna, and M. Castilla, "Hierarchical control of droop-controlled ac and dc microgrids x2014;a general approach toward standardization," *IEEE Transactions on Industrial Electronics*, vol. 58, no. 1, pp. 158–172, Jan 2011.

[3] V. Nasirian, S. Moayedi, A. Davoudi, and F. L. Lewis, "Distributed cooperative control of dc microgrids," *IEEE Transactions on Power Electronics*, vol. 30, no. 4, pp. 2288–2303, April 2015.

[4] X. Lu, J. M. Guerrero, K. Sun, and J. C. Vasquez, "An improved droop control method for dc microgrids based on low bandwidth communication with dc bus voltage restoration and enhanced current sharing accuracy," *IEEE Transactions on Power Electronics*, vol. 29, no. 4, pp. 1800–1812, April 2014.

[5] Q. Shafiee, J. M. Guerrero, and J. C. Vasquez, "Distributed secondary control for islanded microgrids x2014;a novel approach," *IEEE Transactions on Power Electronics*, vol. 29, no. 2, pp. 1018–1031, Feb 2014.

[6] R. Han, L. Meng, G. Ferrari-Trecate, E. A. A. Coelho, J. C. Vasquez, and J. M. Guerrero, "Containment and consensus-based distributed coordination control to achieve bounded voltage and precise reactive power sharing in islanded ac microgrids," *IEEE Transactions on Industry Applications*, vol. 53, no. 6, pp. 5187–5199, Nov 2017.

[7] H. Wang, M. Han, R. Han, J. Guerrero, and J. Vasquez, "A decentralized current-sharing controller endows fast transient response to parallel dc-dc converters," *IEEE Transactions on Power Electronics*, vol. PP, no. 99, pp. 1–1, 2017.

[8] J. W. Simpson-Porco, Q. Shafiee, F. Dörfler, J. C. Vasquez, J. M. Guerrero, and F. Bullo, "Secondary frequency and voltage control of islanded microgrids via distributed averaging," *IEEE Transactions on Industrial Electronics*, vol. 62, no. 11, pp. 7025–7038, Nov 2015.

[9] V. Nasirian, Q. Shafiee, J. M. Guerrero, F. L. Lewis, and A. Davoudi, "Droop-free distributed control for ac microgrids," *IEEE Transactions on Power Electronics*, vol. 31, no. 2, pp. 1600–1617, Feb 2016.

[10] R. Han, H. Wang, Z. Jin, L. Meng, and J. M. Guerrero, "Containment-based distributed coordination control to achieve both bounded voltage and precise current sharing in reverse-droop-based dc microgrid," in *2017 IEEE Energy Conversion Congress and Exposition (ECCE)*, Oct 2017, pp. 4121–4127.